# Study of the press forming mechanism of a thermoforming machine

Belforte G, Colombo F, Maffiodo D and Raparelli T
*Department of Mechanical and Aerospace Engineering, Politecnico di Torino, Italy*

*Keywords:* mechanism, cam synthesis, dynamics, thermoforming machine

**Abstract**

The paper presents kinematic and dynamic investigations of the main press forming mechanism of a thermoforming machine.

A multibody analysis of this press forming mechanism, which lifts and rotates a press bed, was carried out. Press bed lifting, which is necessary to form the component, is performed by means of a first rod and toggle mechanism. Press bed rotation to eject the formed component is produced by means of a second rod and must be appropriately shifted. These rods are oscillating followers driven by cams, making it possible to precisely define trajectories as a function of the motor shaft rotation angle.

Analysis is performed by numerically solving the equations of motion. Cam synthesis on the basis of the oscillating followers' trajectories makes it possible to obtain cam profiles in order to evaluate pressure angles and check that there is no undercutting.

System dynamics is investigated in order to evaluate motor torque and analyze internal stresses on the hinges. In addition, some experimental results and those obtained with the dynamic model are compared. Performance improvement of the actual machine is carried out by modifying the trajectory of the press bed by means of a numerical code at the purpose developed. This approach is more

convenient than the use of a commercial multibody code, that is not specifically built for parametric studies.

## INTRODUCTION

There are two main ways of performing functional design of complex mechanical systems: the first consists of modelling by means of commercial multibody codes, while the second entails solving the equations of motion numerically by means of codes developed for the purpose**.**

Commercial and open multibody codes are now widely used for industrial research and functional design because they combine efficiency, reliability and visual effectiveness for many categories of mechanical system models. On the other hand, the use of these codes can lead to difficulties in optimizing systems and evaluating results. This approach calls for defining and managing a large number of parameters. The alternative approach requires a custom numerical code development, but provides greater opportunities for studying a mechanism in depth [1,2].

In view of these considerations, the investigation described herein was carried out with this second approach. In addition, the analytical parametric study of cam mechanisms was particularly useful for the design of new improved devices. Many papers on this topic can be found in literature. For example, Nishioka [3] investigated parallel cam mechanisms with a parametric configuration which can cover every configuration, developing a new internal parallel mechanism having a large angular stroke of output in a limited space.

Wu [4] presents an analytical approach for determining the profiles of conjugate disc cams in the form of parametric vector equations. His approach is based on the principle that the contact points between the conjugate cam and the follower can be determined according to the locations of instantaneous centres of zero velocity and follower position.

A particular kind of cam with circular arc profiles was studied by Lanni et al. [5] with an algebraic approach in order to overcome the limitations of graphical techniques. These cams are useful for low cost transmissions because of their simple machining, but can only be employed for low speed applications because of their discontinuous acceleration diagram.

Balkwill and Morrey [6] developed two methods for modelling a rotationally flexible cam drive in a simplified way, using their models to predict system performance. A major limit is the linear damping hypothesis, which introduces significant errors.

To evaluate whether the motion of the entire mechanism can be optimized, polynomials can be used to impose different trajectories and to simulate its behaviour. Hwang and Yu [7] used this technique for the adjustable knock-out cam-follower mechanism of a bolt former.

The specific problem of size optimization of a cam mechanism with a translating roller follower is solved by Yu and Lee [8] using a non-linear programming technique and a family of parametric polynomials.

This paper addresses the functional design of the main press forming mechanism of a thermoforming machine, evaluating the machine's performance and kinematic and dynamic characteristics. Functional design is performed with a numerical method implemented in Matlab software. This choice was made to facilitate mechanism design and to improve the performance of the system.

## DESCRIPTION OF THE MACHINE

The system under study is the mechanism of a thermoforming machine for plastic glasses. During the forming operation, the press bed (1) is moved by the mechanism described herein in order to accomplish its tasks. Figure 1 shows the mechanism that moves the press bed, represented in a generic position. There are two pairs of conjugate cams secured to the camshaft. Pair (2) drives the press bed

vertical displacement via a pair of rocker arms (3) connected to rod (4) at (A). The other end (B) of the rod is connected to a toggle (5) which can rotate about a fixed hinge (O2). A moving hinge at (C) connects this element to a rod (6), whose end (D) is hinged to the press bed (1). Two slideways (7) guide the press bed during its displacement. Paired cams (8) drive rotation of the press bed (1) by means of a pair of rocker arms (9) and rod (10), which ends directly with its hinge (F) on the press bed.

The shape of the first pair of cams determines the press bed vertical motion, while the shape of the second pair determines its rotation. The relationship between the two motions determines the entire motion of the press bed, whose task is to form a battery of glasses; this relationship depends on the relative angular positioning of the two pairs of cams.

The machine cycle consists of the following stages:

- Thermoforming
- Cutting from the plastic sheet stock
- Ejection

Specifically, the press bed in which the glasses are formed is moved along a closed trajectory from the forming position to the ejection position. During the forming stage, the press bed must be fixed horizontally, after which it must be moved downwards and rotated to eject the formed glasses. The rotation angle of the press bed between forming and ejection is $\alpha_{max}=80°$.

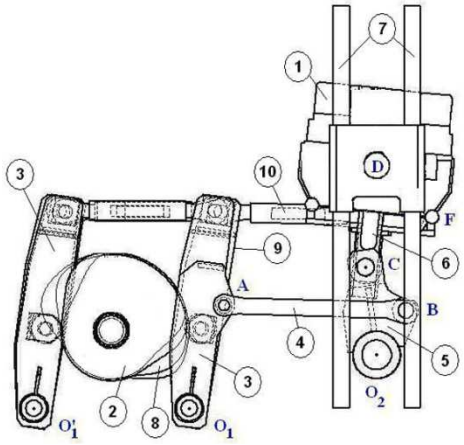


Figure 1: Sketch of the mechanism that moves the press bed.

**NUMERICAL MODEL**

The mechanism (figure 2) presents two degrees of freedom. The motion can be described by the following input trajectories, defined versus the cam shaft angle $\vartheta$:

- angle $\vartheta_1(\vartheta)$ of the vertical translation follower and
- angle $\vartheta_2(\vartheta)$ of the rotation follower

Given the coordinates of fixed hinges $O_1$, $O_2$ and the initial positions of hinges A, B, C, D, E and F, the direct kinematics is solved with the algorithm described hereunder.

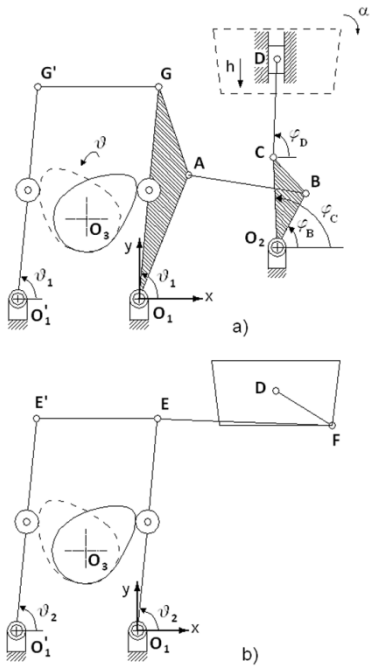


Figure 2: Sketch of the mechanism in the starting position: a) vertical translation follower mechanism; b) rotation follower mechanism.

**Forward kinematics**

The forward kinematics makes it possible to obtain the die trajectory on the base of the input follower rotation trajectories $\vartheta_1(\vartheta)$ and $\vartheta_2(\vartheta)$. The die trajectory is expressed by the vertical displacement $h(\vartheta)$ of hinge D and the rotation angle $\alpha(\vartheta)$ (see figure 1).

For each cam shaft angle $\vartheta$, the position of hinges A and E are calculated with simple trigonometric relations. The coordinates of hinge B are obtained from the intersection of the circles centered in $O_2$ with radius $O_2B$ and the circle centered in A of radius AB. The algorithm adopted calculates two solutions and selects the correct one on the base of the followers' position. The procedure is repeated

for hinges C, D and F. Finally, the vertical displacement and the rotation of the press bed are expressed as

$$h(\vartheta) = y_D(\vartheta) - y_D(0) \tag{1}$$

$$\alpha(\vartheta) = atan\left(\frac{y_D(\vartheta) - y_F(\vartheta)}{x_D(\vartheta) - x_F(\vartheta)}\right) - atan\left(\frac{y_D(0) - y_F(0)}{x_D(0) - x_F(0)}\right) \tag{2}$$

The elements' centres of mass coordinates $x_G$, $y_G$ are then calculated on the base of the hinges coordinates $x_{A\text{-}F}$, $y_{A\text{-}F}$.

Given the constant rotational speed of the cam shaft $\omega$, the time functions $x(t)$ and $\varphi(t)$ can be obtained with the relation $\vartheta = \omega t$, while the time derivatives (as e.g. $\dot{x}$ and $\ddot{x}$) can be related to the geometric derivatives (as e.g. $x'$ and $x''$) by:

$$\dot{x} = \frac{d\vartheta}{dt}\frac{dx}{d\vartheta} = \omega\frac{dx}{d\vartheta} = \omega x', \quad \dot{\varphi} = \omega\frac{d\varphi}{d\vartheta} = \omega\varphi' \tag{3}$$

$$\ddot{x} = \omega^2\frac{d^2x}{d\vartheta^2} = \omega^2 x'', \quad \ddot{\varphi} = \omega^2\frac{d^2\varphi}{d\vartheta^2} = \omega^2\varphi'' \tag{4}$$

Central finite difference discretization is used to calculate the geometric derivatives of functions x($\vartheta$) and $\varphi(\vartheta)$.

**Inverse kinematics**

The inverse kinematics is used to obtain the followers' trajectories $\vartheta_1(\vartheta)$ and $\vartheta_2(\vartheta)$ on the basis of the press bed input trajectories $h(\vartheta)$ and $\alpha(\vartheta)$ of the press bed. This is done with a procedure analogous to the one used in forward kinematics. The rotations of the followers are then obtained:

$$\vartheta_1(\vartheta) = atan\left(\frac{y_A(\vartheta) - y_{O1}}{x_A(\vartheta) - x_{O1}}\right) \tag{5}$$

$$\vartheta_2(\vartheta) = atan\left(\frac{y_E(\vartheta) - y_{O1}}{x_E(\vartheta) - x_{O1}}\right) \tag{6}$$

**Cam synthesis**

Cam synthesis can be used to obtain the cam profiles when the trajectory of the follower is defined. The cam profile depends on follower geometry (follower length $O_1S$ and roller radius $R_r$), on the distance $O_1O_3$ from the centre of the cam (see figure 3), and on the trajectory established for the follower. Given the functions $\vartheta_1(\vartheta)$ and $\vartheta_2(\vartheta)$, the radial coordinate *r* of the principal cams is calculated as a function of the contact angle $\xi$ in polar coordinates with the following parametric relations [10]:

$$r = \sqrt{(O_1S\ sin\beta - R_r sin\psi)^2 + (O_1O_3 - O_1S\ cos\beta - R_r cos\psi)^2} \tag{7}$$

$$\beta = \frac{3\pi}{4} - \vartheta_1 \tag{8}$$

$$\psi = \tan^{-1}\frac{O_1S\ sin\beta\left(1 + \frac{\partial\vartheta_1}{\partial\vartheta}\right)}{O_1O_3 - O_1S\ cos\beta\left(1 + \frac{\partial\vartheta_1}{\partial\vartheta}\right)} \tag{9}$$

The contact angle $\xi$ is related to the input shaft angle $\vartheta$ by

$$\xi = \vartheta + \alpha_P - \pi/4 \tag{10}$$

where

$$\alpha_P = \tan^{-1}\frac{O_1S\ sin\beta - R_r sin\psi}{O_1O_3 - O_1S\ cos\beta - R_r cos\psi} \tag{11}$$

In order to calculate the profile of the conjugate cams, equations (7-11) were modified on the basis of the definition of angles $\alpha_P{}'$, $\beta'$, $\xi'$ (see figure 3) as follows:

$$r' = \sqrt{(O_1S'sin\beta' - R_r sin\psi')^2 + (O_1{}'O_3 - O_1{}'S'cos\beta' - R_r cos\psi')^2} \tag{12}$$

$$\beta' = \vartheta_1 - \pi/4 \tag{13}$$

$$\psi' = \tan^{-1}\frac{O_1{}'S'\, sin\beta'\left(1 - \frac{\partial\vartheta_1}{\partial\vartheta}\right)}{O_1{}'O_3 - O_1{}'S'\, cos\beta'\left(1 - \frac{\partial\vartheta_1}{\partial\vartheta}\right)} \tag{14}$$

$$\xi' = \vartheta - \alpha_P' + 5\pi/4 \tag{15}$$

$$\alpha_P{}' = \tan^{-1}\frac{O_1{}'S'sin\beta' - R_r sin\psi'}{O_1{}'O_3 - O_1{}'S'\, cos\beta' - R_r cos\psi'} \tag{16}$$

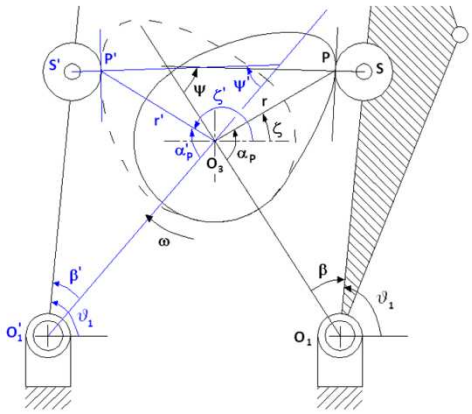


Figure 3: Sketch of the cam and follower system

**Dynamics**

The system dynamics is solved by means of two approaches: the Newtonian and the Lagrangian approach. In the Newtonian approach, the forces on constraints, the inertial terms and the external forces are considered for each element. An example of a free body diagram is given in figure 4.

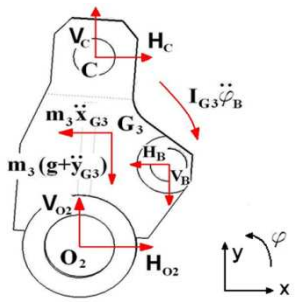


Figure 4: Free body diagram of element $O_2BC$

The dynamic equations obtained by the balance of forces and moments applied to each body are organized in the following matrix relation:

$$[A]\{R\} = \{F_i\} + \{F_e\} \tag{17}$$

where $\{R\}$ is the vector of the reactions in constraints and $\{F_i\}$ and $\{F_e\}$ are the inertial terms and the external forces respectively. The inertial terms are calculated with the following equation,

$$\{F_i\} = -[M]\{\ddot{X}_G\} \tag{18}$$

in which the centres of mass coordinates and angular positions are organized in vector $\{X_G\}$ and the masses and moments of inertia in matrix $[M]$.

Matrix [*A*] has non-constant coefficients, being a function of coordinates $x_i$ and $\varphi_i$. The differential algebraic equations system (17) is solved iteratively for each value of the cam shaft angle $\vartheta$.

Calculations are also performed with the Lagrangian approach by simply equating the input torque to the geometric derivative of the total energy. Applying the work-energy equation to the cinematism and performing the time derivative to both members one obtains:

$$\frac{dL}{dt} = \omega \frac{dL}{d\vartheta} = \omega \frac{d}{d\vartheta} \sum_i \left( \frac{1}{2} m_i \left( \dot{x}_{Gi}{}^2 + \dot{y}_{Gi}{}^2 \right) + \frac{1}{2} I_{Gi} \dot{\varphi}_i{}^2 + m_i g y_{Gi} \right)$$

where the contributions of translational and rotational kinetic energies and gravitational energy for each element *i* are evident.

The use of geometric derivatives allows to investigate the torque contributions independently on the angular speed $\omega$ of the input shaft. In particular, if the inertia of all bodies is neglected with respect to the inertia of the press bed, the equation that expresses the torque becomes:

$$C = m\omega^2 (x'_G x''_G + y'_G y''_G) + I_G \omega^2 \varphi' \varphi'' + m g y'_G \tag{19}$$

where parameters $m, I_G, x_G, y_G, \varphi$ are referred to the press bed.

This equation expresses well the relationship between the kinematic parameters and the torque.

The input torques calculated with the two methods are compared in figure 5: the assumption whereby only the mass of the press bed is considered provides a good approximation because the relative error is less than 3%.

a)

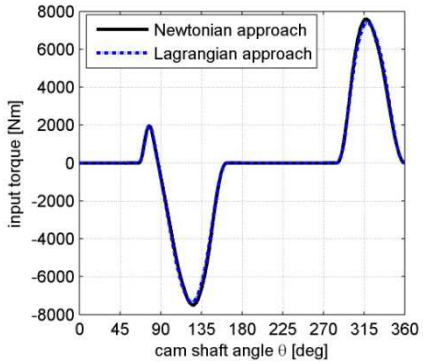


b)

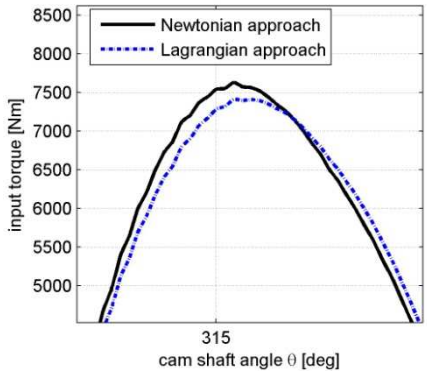


Figure 5: a) Input torque; comparison between the Newtonian approach and the Lagrangian approach; in the second case only the inertia of the press bed is considered; b) details of the torque

**EXPERIMENTAL VALIDATION**

Figure 6 shows experimental torque on the input shaft for different rotation speeds. Torque is evaluated by measuring the current absorbed by the synchronous motor controlled in closed speed loop at a sampling rate of 2 kHz. A speed reducer is installed between the motor and the input shaft. Tests were carried out without the plastic sheet stock used to form the glasses (no forming).

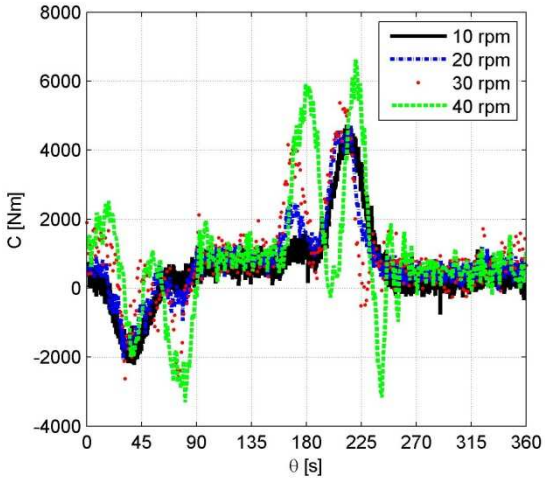


Figure 6: Experimental torque on input shaft at 10, 20, 30 and 40 rpm.

Figure 7 compares the experimental motor torque and the numerical torque at 10 and 40 rpm respectively. The numerical model considers rigid bodies and neglects possible compliances, which in the actual situation cause the press bed trajectory to differ from the ideal case. Friction is also not considered in the numerical model, so that torque differs from that determined experimentally. This is clear during the stage in which the press bed rises from the bottom to the top position.

a)

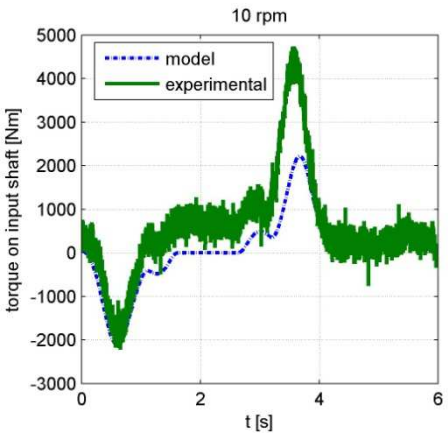


b)

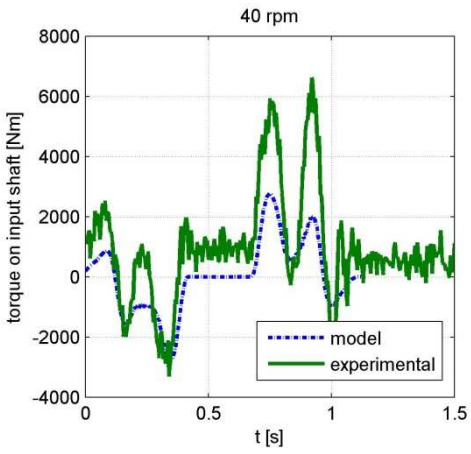

Figure 7: Experimental torque on input shaft at 10 and 40 rpm; comparison between theoretical and experimental results

## PERFORMANCE IMPROVEMENT

After the validation of the numerical code, this was used to design a new machine, able to produce an increased number of glasses for each cycle. Performance improvement was carried out in order to reduce motor torque.

The following parameters were maintained constant in defining the trajectories:

- die rotation $\alpha_{max}$,
- die vertical displacement $h_{max}$ and
- cam angles $\vartheta_S$ and $\vartheta_R$ corresponding to press bed translation and rotation.

Table 1 shows the phases of the cycle and the corresponding cam angles for translation and rotation mechanisms.

Table 1: phases of the cycle and the corresponding cam angles

| **angle θ (deg)** | **translation** | **rotation** |
|---|---|---|
| 355 | thermoforming and cutting | |
| 94 | downstroke motion | |
| 121 | | clockwise rotation |
| 160 | | |
| 192 | ejection | |
| 253 | | counterclockwise rotation |
| 288 | upstroke motion | |
| 324 | | |

Trajectories $h(\vartheta)$ and $\alpha(\vartheta)$ were defined by specifying the coordinates of six points (Figure 8, A to F and A' to F') equally spaced along axis $\vartheta$. Considering the press bed translation, for example, the equations imposed are:

$$h(\vartheta_{A-F}) = h_{A-F} \tag{20}$$

Continuity of velocity and acceleration was imposed at points A and F:

$$\left|\frac{\partial h}{\partial \vartheta}\right|_{A-} = \left|\frac{\partial h}{\partial \vartheta}\right|_{A+}; \quad \left|\frac{\partial h}{\partial \vartheta}\right|_{F-} = \left|\frac{\partial h}{\partial \vartheta}\right|_{F+} \tag{21}$$

$$\left|\frac{\partial^2 h}{\partial \vartheta^2}\right|_{A-} = \left|\frac{\partial^2 h}{\partial \vartheta^2}\right|_{A+}; \quad \left|\frac{\partial^2 h}{\partial \vartheta^2}\right|_{F-} = \left|\frac{\partial^2 h}{\partial \vartheta^2}\right|_{F+} \tag{22}$$

The phase shift between the two trajectories $\varphi_{SR} = \vartheta_{A'} - \vartheta_A$ can also be changed during the performace improvement.

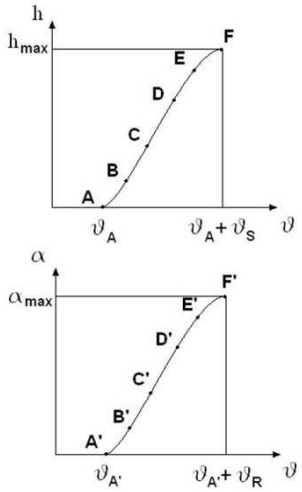


Figure 8: Scheme of the trajectories $h(\vartheta)$ and $\alpha(\vartheta)$

Considering these constraints the trajectory is represented by a polynomial curve of degree 9:

$$h(\vartheta) = c_0 + c_1\vartheta + c_2\vartheta^2 + c_3\vartheta^3 + c_4\vartheta^4 + c_5\vartheta^5 + c_6\vartheta^6 + c_7\vartheta^7 + c_8\vartheta^8 + c_9\vartheta^9 \tag{23}$$

The coefficients $c_0$-$c_9$ are obtained by solving the system:

$$\begin{bmatrix} 1 & \vartheta_A & \vartheta_A^2 & \vartheta_A^3 & \dots & \vartheta_A^9 \\ 1 & \vartheta_B & \vartheta_B^2 & \vartheta_B^3 & & \vartheta_B^9 \\ \vdots & & & & & \\ 1 & \vartheta_F & \vartheta_F^2 & \vartheta_F^3 & & \vartheta_F^9 \\ 0 & 1 & 2\vartheta_A & 3\vartheta_A^2 & & 9\vartheta_A^8 \\ 0 & 1 & 2\vartheta_F & 3\vartheta_F^2 & & 9\vartheta_F^8 \\ 0 & 0 & 2 & 6\vartheta_A & & 72\vartheta_A^7 \\ 0 & 0 & 2 & 6\vartheta_F & & 72\vartheta_F^7 \end{bmatrix} \begin{Bmatrix} c_0 \\ c_1 \\ \vdots \\ c_9 \end{Bmatrix} = \begin{Bmatrix} h_A \\ h_B \\ \vdots \\ h_F \\ 0 \\ 0 \\ 0 \\ 0 \end{Bmatrix} \tag{24}$$

The downstroke and the upstroke trajectories were considered symmetrical. The same calculations were done for rotation $\alpha(\vartheta)$.

To improve the performance of the machine the torque due to rotation was considered at first, as it is the most important contribution. Given the position of points A' and F' (determined by the operating phases of the machine) the position of the other points was changed. The points were chosen equispaced along θ axis. The vertical coordinates of points D and E were related to that of points B and C by:

$$\begin{aligned} \alpha_{D'} &= \alpha_{max} - \alpha_{C'} \\ \alpha_{E'} &= \alpha_{max} - \alpha_{B'} \end{aligned} \tag{25}$$

For different positions of point B', the position of point C' that better reduces the torque was found. Figure 9 and 10 compare these best rotational torque contributions and trajectories obtained with this

procedure. In all calculations the cam shaft rotates at 40 rpm. It can be noticed that the torque was reduced of about three times with a slight change in the trajectory.

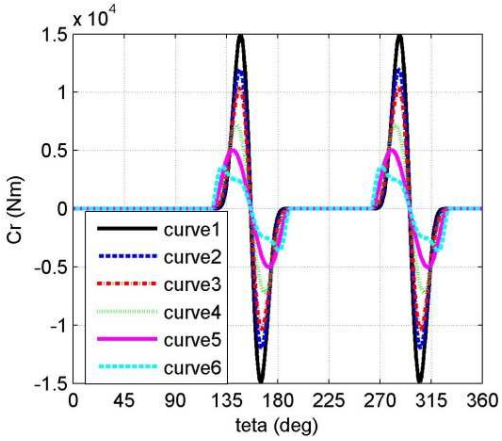


Figure 9: Rotational torque $C_r$ vs shaft angle $\theta$; comparison between the best curves obtained

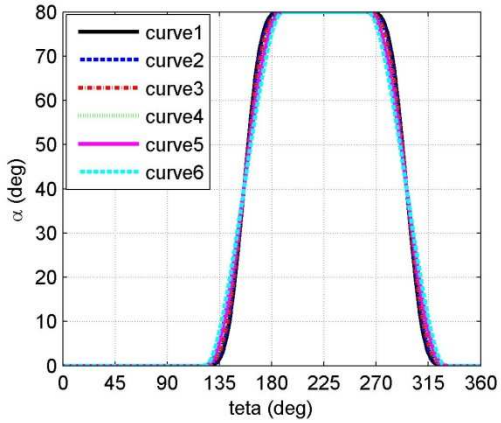


Figure 10: Rotational trajectories corresponding to the best curves obtained

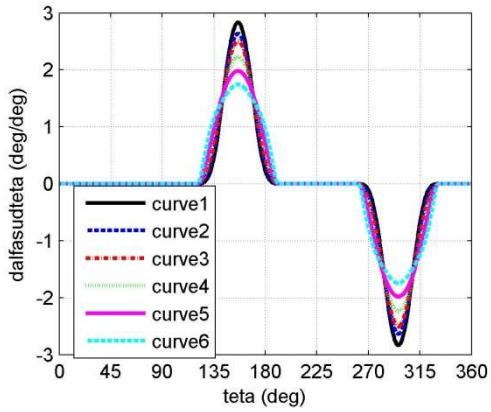


Figure 11: Angular speed corresponding to the best curves obtained

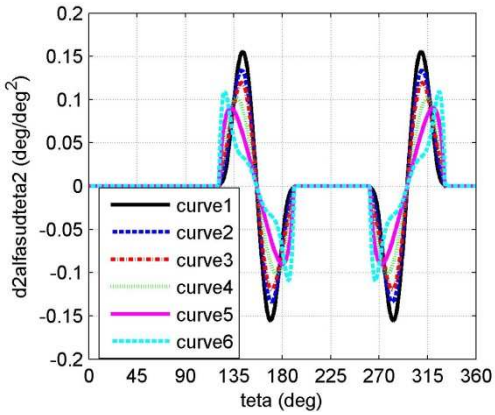


Figure 12: Angular acceleration corresponding to the best curves obtained

As the integral of Cr represents a difference of rotational kinetic energy, if the maximum rotational speed is decreased, also the positive area of the region bounded by the torque curve decreases. There is a limit in decreasing this maximum speed as the press bed must be rotated of $\alpha_{max}$ in a given cam shaft angle. As the maximum speed approximates the average speed (see figure 11), the initial slope increases and the torque begins to oscillate. Augmented acceleration (figure 12) can cause vibration problems on

the machine. It is evident that the best solution can be obtained with a compromise between torque decrease and limitation of the acceleration.

The same procedure can be repeated for the translation trajectory to decrease the corresponding torque contribution.

Figure 13 depicts the three torque contributions of equation (18) due to variation in the rotational and translational kinetic energies and the gravitational energy of the press bed. In this figure, curve 6 is considered. The torque contributions partially compensate each other. In particular it is possible to take advantage of this compensation during the first half of the press bed downstroke motion, while in the second half all contributions are negative. In the latter case there is no possibility to decrease the maximum negative torque. Analogous considerations can be done for the upstroke motion.

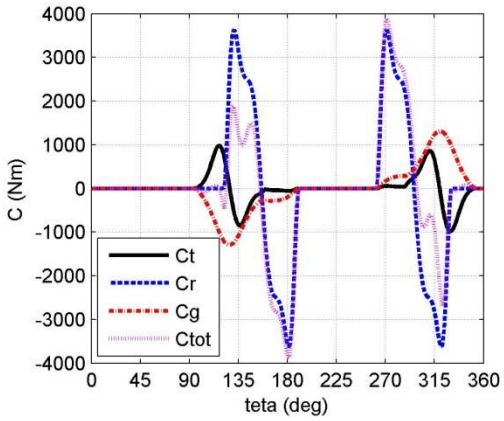


Figure 13: Torque contributions due to variation in the rotational and translational kinetic energies and the gravitational energy

## CONCLUSIONS

Functional design of the main press forming mechanism of a thermoforming machine was performed with a lumped parameters multibody numerical model based on Matlab language.

At first the model was validated with experimental results carried out on an existing machine, then it was used to perform the design of a new bigger machine, improving its performance.

There are three contributions to the motor torque: the translational one, the rotational one and the gravitational one. The main contribution is the rotational one; this was decreased of about three times by modifying the rotational trajectory. The reduction of the maximum torque was limited by the maximum allowed acceleration to contain the vibrations induced to the machine. As the different torque contributions partially compensate each other, a performance improvement based on phase shift can be considered, but this is limited by machine operating specifications. Moreover it is possible to take advantage of each torque contribution compensation only during the first half of the press bed downstroke motion, as in the second half all contributions are negative. In this case there is no possibility to decrease the maximum negative torque.

## REFERENCES

[1] R. Norton, “Cam design and manufacturing handbook”, 2nd edition, New York, NY, Industrial Press Inc., 2009.

[2] H. Eckhardt, “Kinematics design of machines and mechanisms”, New York, NY, McGraw Hill, 1998.

[3] Nishioka M, Nishimura T, “Syntesis of the internal parallel cam mechanism”, Proceedings of the Institution of Mechanical Engineers, Part C: Journal of Mechanical Engineering Science 1998, vol 212, pag 577-585.

[4] Wu L-I, “Calculating conjugate cam profiles by vector equations”, Proceedings of the Institution of Mechanical Engineers, Part C: Journal of Mechanical Engineering Science 2003, vol 217, pag 1117-1123.

[5] Lanni C, Carbone G, Ceccarelli M, Ottaviano E, “Numerical and experimental analyses of radial cams with circular-arc profiles”, Proceedings of the Institution of Mechanical Engineers, Part C: Journal of Mechanical Engineering Science 2006, vol 220, pag 761-774.

[6] Balkwill JDG, Morrey D, “Dynamic analysis of rotationally flexible cam mechanisms” Proceedings of the Institution of Mechanical Engineers, Part C: Journal of Mechanical Engineering Science 1999, vol 213, pag 537-550.

[7] Hwang W M, Yu Q, , “Optimal synthesis of the adjustable knock-out cam-follower mechanism of a bolt former”, Proceedings of the Institution of Mechanical Engineers, Part C: Journal of Mechanical Engineering Science 2006, vol 219, pag 767-774.

[8] Yu Q, Lee H P, “Size optimization of cam mechanisms with translating roller followers”, Proceedings of the Institution of Mechanical Engineers, Part C: Journal of Mechanical Engineering Science 1998, vol 212, pag 381-386.

[9] Lin W Y, Hsiao K M, “Study on improvements of the five-point double-toggle mould clamping mechanism”, Proceedings of the Institution of Mechanical Engineers, Part C: Journal of Mechanical Engineering Science 2004, vol 218, pag 761-774

[10] Magnani L., Ruggeri G., “Meccanismi per macchine automatiche”, Torino, Italy, Utet, 1986.

**APPENDIX**

Notation

| | |
|---|---|
| $\alpha$ | press bed clockwise rotation |
| $h$ | press bed vertical displacement |
| $\theta$ | cam shaft angle |
| $\theta_1$ | angle of the translation follower |
| $\theta_2$ | angle of the rotation follower |
| $x, y$ | cartesian coordinates |
| $x_{Gi}, y_{Gi}$ | coordinates of the center of mass of element $i$ |
| $\varphi_i$ | counterclockwise rotation of element $i$ |
| $\omega$ | speed of rotation of the cam shaft |

| | |
|---|---|
| $R_r$ | roller radius |
| $r$ | radius of the principal cam |
| $r'$ | radius of the conjugate cam |
| $\zeta$ | contact angle of the principal cam |
| $\zeta'$ | contact angle of the conjugate cam |
| $L$ | mechanical work |
| $C$ | torque on the input cam shaft |
| $g$ | gravitational acceleration |
| $m_i$ | mass of element *i* |
| $I_{Gi}$ | mass moment of inertia of element *i* calculated with respect to its center of mass |
| $\theta_S$ | cam angle of vertical motion |
| $\theta_R$ | cam angle of rotation motion |
| $\varphi_{SR}$ | phase shift between vertical motion and rotation motion |